

Available online at www.sciencedirect.com

ScienceDirect

www.elsevier.com/locate/jmbbm

Research Paper

Histo-mechanical properties of the swine cardinal and uterosacral ligaments

Ting Tan^a, Frances M. Davis^a, Daniel D. Gruber^b, Jason C. Massengill^c,
John L. Robertson^a, Raffaella De Vita^{a,*}

^aDepartment of Biomedical Engineering and Mechanics, Virginia Tech, Blacksburg, VA 24061, USA

^bDepartment of Obstetrics and Gynecology, Walter Reed National Military Medical Center, Bethesda, MD 20814, USA

^cDepartment of Urogynecology, Wright-Patterson Medical Center, Ohio, OH 45433, USA

ARTICLE INFO

Article history:

Received 15 August 2014

Received in revised form

7 November 2014

Accepted 18 November 2014

Keywords:

Uterosacral ligament

Cardinal ligament

Tensile properties

SEM

Histology

Mechanical testing

ABSTRACT

The focus of this study was to determine the structural and mechanical properties of two major ligaments that support the uterus, cervix, and vagina: the cardinal ligament (CL) and the uterosacral ligament (USL). The adult swine was selected as animal model. Histological analysis was performed on longitudinal and cross sections of CL and USL specimens using Masson's trichrome and Verhoeff–van Giesson staining methods. Scanning electron microscopy was employed to visualize the through-thickness organization of the collagen fibers. Quasi-static uniaxial tests were conducted on specimens that were harvested from the CL/USL complex of a single swine. Dense connective tissue with a high content of elastin and collagen fibers was observed in the USL. Loose connective tissue with a considerable amount of smooth muscle cells and ground substance was detected in both the CL and USL. Collagen fibers, smooth muscle cells, blood vessels, and nerve fibers were arranged primarily in the plane of the ligaments. The USL was significantly stronger than the CL with higher ultimate stress and tangent modulus of the linear region of the stress–strain curve. Knowledge about the mechanical properties of the CL and USL will aid in the design of novel mesh materials, stretching routines, and surgical procedures for pelvic floor disorders.

© 2014 Elsevier Ltd. All rights reserved.

1. Introduction

Pelvic floor disorders (PFDs) such as urinary incontinence, fecal incontinence, and pelvic organ prolapse affect millions of women every year. These disorders, which are mainly caused by pregnancy, vaginal delivery, and aging (MacLennan et al., 2000; Kepenekci et al., 2011), have devastating consequences not only on the quality of life of women but also the healthcare system (Kenton and Mueller, 2006). The annual direct cost of

prolapse surgeries alone exceeds 1 billion dollars in the United States (Subak et al., 2001). The burden placed by PFDs on women and the healthcare system will become even more significant with the projected increase in the aging population. Indeed, it has been estimated that the number of American adult women who suffer for PFDs will rise from 28.1 million in 2010 to 43.8 million in 2050 (Wu et al., 2009).

PFDs occur due to structural and mechanical alterations of pelvic organs, muscles, ligaments, and fasciae. Recent studies

*Corresponding author.

E-mail address: devita@vt.edu (R. De Vita).

have suggested that “problems of bladder, bowel, prolapse, and some types of pelvic pain, mainly originate from the vaginal ligaments, not from the organs themselves (Petros, 2010).” The vaginal ligaments are mainly composed of collagen fibers interlaced with elastin, smooth muscle cells, nerve fibers, fibroblasts, and vascular structures. During pregnancy and childbirth, these ligaments are likely to lose their strength and increase their laxity due to the release of relaxin, a placental hormone that reduces the production of collagen and increases collagen breakdown (Sherwood, 2004). The mechanical properties of the entire vagina/supportive ligaments complex have been shown to be restored after parturition (Lowder et al., 2007). However, in many cases, the structure of the ligaments is permanently altered due to childbirth trauma and, consequently, their mechanical function is likely to be compromised. With menopause and aging, elastin and collagen degradation may also lead to laxity of the vaginal ligaments (Ewies et al., 2003; Goepel, 2008; Chen et al., 2002). These morphological changes in the ligaments are, most probably, linked to a reduction in estrogen (Mokrzycki et al., 1997).

The two major suspensory ligaments of the uterus, cervix, and vagina are the uterosacral ligament (USL) and the cardinal ligament (CL) located in a posterior direction over the levator plate of the pelvic diaphragm. The USL provides support to the cervix and the upper vagina and is connected to the sacrum (DeLancey, 1994; Buller et al., 2001; Amundsen et al., 2003). Pelvic pain in pregnancy, nocturia, urgency, and abnormal bladder emptying are believed to be caused by the laxity of the USL (Petros, 2010). The CL is linked to the USL at the cervix and extends to the upper fascia of the pelvis. Prolapse of the vagina and uterus has been associated with the laxity of both USL and CL (Miklos et al., 2002; Petros, 2010).

The importance of investigating the biomechanical properties of the USL and CL for the treatment of PFDs has been recognized only in the past few years (Weber et al., 2004). Force and displacement data have been collected on the ligaments by employing different techniques (Reay Jones et al., 2003; Cosson et al., 2003; Moalli et al., 2005), including *in-vivo* measurement methods (Luo et al., 2014). These data are, however, highly dependent on the dimensions of the tested specimens. Consequently, the biomechanical properties computed from them cannot be generalized to specimens of different dimensions. Stress and strain data have been collected to characterize the elasticity and viscoelasticity of USLs via uniaxial tests (Vardy et al., 2005; Martins et al., 2013; Rivaux et al., 2013) and of USLs and CLs via biaxial tests (Becker and De Vita, 2014). These data describe the mechanical behavior of USL and CL, independently of their size. In the experimental study by Vardy et al. (2005), quasi-static tensile tests and incremental stress relaxation tests of USLs from monkeys were performed, demonstrating their non-linear elasticity and viscoelasticity. The study by Vardy et al. (2005) is notable for being the first attempt to determine the mechanical behavior of USLs. Tensile properties such as ultimate tensile strength and stiffness of female cadaveric USLs were computed for the first time by Martins et al. (2013). In the study by Martins et al. (2013), stress and strain data were reported, although strain data were computed from the clamp displacement (and not using more accurate video strain measurement methods). Mooney–Rivlin constitutive

parameters were employed by Rivaux et al. (2013) to quantify the nonlinear elasticity of female cadaveric USLs that were uniaxially tested. Biaxial elastic and viscoelastic material properties were computed very recently by our group for both the swine USL and CL using novel constitutive parameters (Becker and De Vita, 2014).

In this study, we determine both the histological and mechanical properties of the USL and CL using the swine as an animal model. Toward this end, we perform scanning electron microscopy (SEM) and histological studies on specimens isolated from one entire USL/CL complex. We conduct tensile tests on specimens located in different anatomical regions within another entire USL/CL complex. From accurate stress and strain data measurements, tensile properties such as elastic moduli of the toe and linear regions of the stress–strain curve, ultimate tensile strength (UTS), and strain at UTS are computed. We then evaluate a possible relation between the composition and structure of these ligaments and their tensile properties.

2. Material and methods

2.1. Harvesting technique

Two full term sows (weights = 261 kg and 234 kg) were acquired from a different study in accordance with an approved Virginia Tech IACUC protocol. The sows were euthanized immediately after giving birth (each sow delivered 13 piglets) and their lower abdomen and hindquarter were isolated and firmly secured to a dissection table. In order to identify the vaginal canal, cervix, and uterus, a plastic rod was inserted in the introitus of the vagina (Fig. 1(a)). By using a scalpel, a midline vertical incision was made until the peritoneal cavity was entered. The pubic symphysis was then separated using a hack saw. A rib spreader was utilized to separate the pubic symphysis for access to the vagina and support structures. Using the plastic rod and a scalpel, the vagina, cervix, uterus, and support structures together with the rectum and bladder were extracted from the abdominal cavity as a single complex. This procedure minimized damage to the CL and USL needed in this study (Fig. 1(b)). The bladder and its connective tissues were carefully removed from the vagina–cervix–uterus complex and discarded.

The USL connected the proximal vagina, from the interdigitating pads (cervix in the swine) to the sacrum. Taking care to retain as much of the USL as possible, a scalpel was used to remove it from its attachments to the vagina and sacrum. The CL fanned out laterally from the lateral vagina, through the broad ligament, including the uterine artery and vein, to the pelvic side wall. The CL was also cautiously dissected to preserve its full course (Fig. 1(b) and (c)).

The vagina and the attached USL and CL were then laid flat on a dissection table, and any excess of adipose or muscular tissue was removed from these ligaments. Finally, the USL and CL were separated from the vaginal wall and kept hydrated with phosphate buffered saline (PBS) solution. After dissection, the ligaments were wrapped in plastic and stored at -20°C . Before each mechanical test, SEM or histological analysis as described hereafter, the ligaments were removed from the freezer and allowed to thaw at room temperature for 30 min.

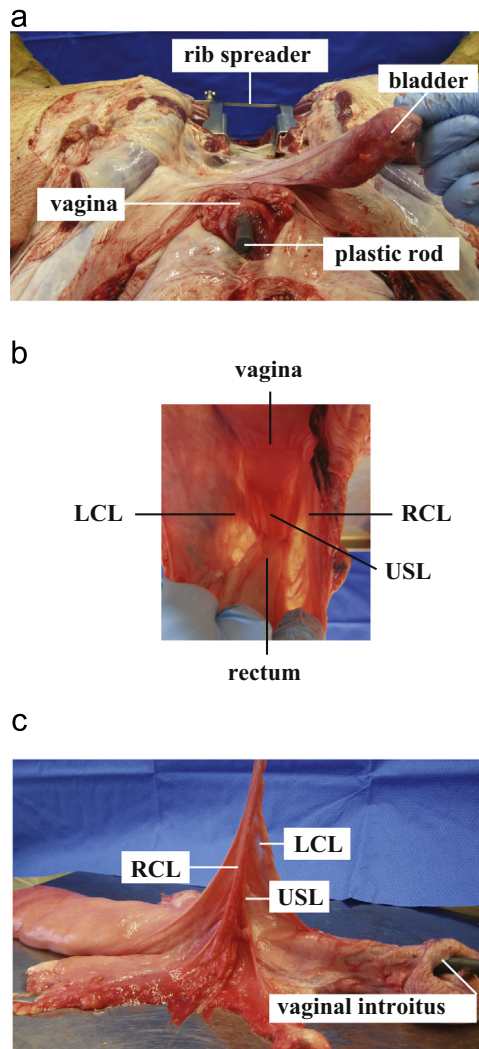


Fig. 1 – (a) Swine peritoneal cavity showing the bladder, vagina, and tools used for dissection. (b) Left cardinal ligament (LCL), uterosacral ligament (USL), and right cardinal ligament (RCL), and their location relative to the rectum and vagina. (c) LCL, USL, and RCL attached to the cervix.

2.2. SEM examination

Specimens collected from the USL and CL of one sow (weight=234 kg) were fixed overnight in a 2% glutaraldehyde–0.01 M sodium cacodylate buffer. They were washed with PBS solution, post-fixed in osmium tetroxide, and dried in a critical point dryer (Model 28000, LADD Research Industries). The specimens were immersed in liquid nitrogen and fractured with a sharp razor blade in order to reveal their cross-sectional area. After being sputter coated with gold, the cross sectional areas were examined using an environmental scanning electron microscope (SEM) (Quanta 600 FEG, FEI).

2.3. Histological examination

The USL and CL excised from one sow (weight=234 kg) were fixed in 10% buffered formalin for 24 h and then stored in 70%

ethanol for 48 h. They were gradually dehydrated in a graded ethanol and xylol series. After dehydration, the specimens were embedded in paraffin wax and cut into 4 μm sections with a microtome. The specimens were stained with Masson's trichrome (MT) or Verhoeff–van Giesson (VVG) stain. Smooth muscle and cytoplasm were stained red and collagen fibers were stained blue using the MT method. Elastin and nuclei were stained black, smooth muscle fibers were stained purple, and collagen fibers were stained pink using the VVG method. The histological slides were examined under a light microscope (Olympus IX71/IX51, Olympus) and images were collected using a digital camera (Model D5000, Nikon) at a 40 \times magnification.

2.4. Uniaxial tensile testing

Uniaxial tensile tests were conducted on a total of 7 specimens isolated from the left CL (LCL), 6 specimens from the right CL (RCL), and 5 specimens from the USL of one sow (weight=261 kg). The specimens were strips approximately 8 mm wide and 80 mm long. These strips were aligned along the main *in-vivo* loading direction of the ligaments as indicated in Fig. 2. Images of each specimen were collected under a stereo-microscope (Stemi 2000C, Zeiss) using a digital camera (Model D5000, Nikon). The width and thickness were measured at six locations using ImageJ (v. 1.44, NIH) and a digital caliper under a 50 g compressive load (Mitutoyo 573-291-20), respectively. The cross-section of each specimen was assumed to be rectangular and its area was calculated using the average width and thickness of the specimen. Four black poppy seeds, serving as fiducial markers for strain measurement, were glued to each specimen. The poppy seeds were evenly spaced on the specimens and were all aligned along the longitudinal axis of the specimens (i.e., the main *in-vivo* loading direction of the ligaments). The ends of each specimen were wrapped in sandpaper and mounted in custom-designed clamps to prevent slippage during mechanical testing.

Uniaxial tensile tests were conducted using an ElectroPuls E1000 (Instron, 50 N load cell) equipped with a bath filled with PBS at room temperature ($\sim 21^\circ\text{C}$). Each specimen was pre-loaded to 0.25 N and preconditioned for five cycles from 0.25 N to 1.0 N at 0.75 mm/s. Five cycles were sufficient to stabilize the response of the specimens. The 0.75 mm/s displacement rate was selected since it was comparable to the displacement rates used in similar studies by other investigators (Vardy et al., 2005; Martins et al., 2013; Rivaux et al., 2013). Following preconditioning each specimen was allowed to recover for 5 min and stretched at 0.75 mm/s until failure occurred. The load and elongation of the specimen were recorded throughout the tests at 10 Hz. In addition, a video camera (APX-RS, Photron) was used to record images of the specimens during testing at 60 Hz with a 512 \times 1024-pixels resolution. The motion of the four poppy seeds was tracked using these images with ProAnalyst (v.1.5.3, Xcitex). The axial Lagrangian strain was then calculated from the motion of the markers. The axial nominal stress was calculated by dividing the load by the initial cross-sectional area.

The axial stress–strain data were analyzed to compute the ultimate tensile strength (UTS) and the strain at the UTS, ϵ_{UTS} . Only uniaxial tests in which the specimens failed in their middle region, away from the clamps, were considered successful.

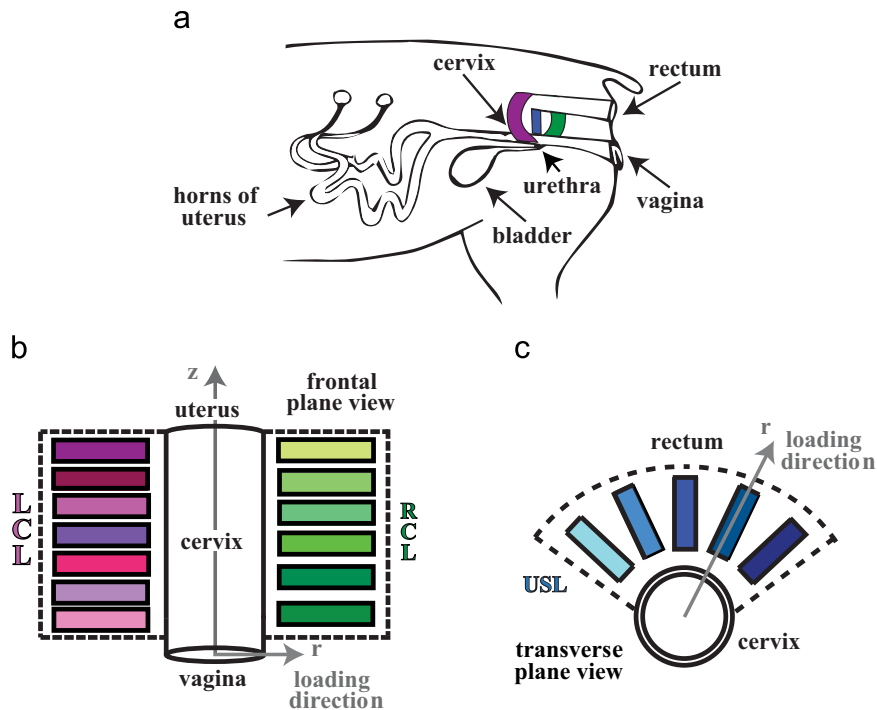


Fig. 2 – (a) Swine reproductive organs and *in-vivo* loading directions of the USL (in blue), RCL (in pink), and LCL (in green). (b) LCL and RCL specimens and their location relative to the vagina/cervix/rectum (frontal plane view). (c) USL specimens and their location relative to the rectum/cervix (transverse plane view). (For interpretation of the references to color in this figure caption, the reader is referred to the web version of this paper.)

The tangent moduli of the toe and linear regions of each stress–strain curve were also computed using simple linear regression. In the toe region, the tangent modulus was calculated by considering only the stress–strain data in the strain interval $[0, 10\% \epsilon_{UTS}]$ while, in the linear region, was computed by considering only the stress–strain data in the interval $[30\% \epsilon_{UTS}, \epsilon_{UTS}]$. Although the choice of these intervals was arbitrary, it provided a consistent method for computing the tangent moduli for the different stress–strain curves.

2.5. Statistical analysis

Mean and standard deviation were calculated for the elastic moduli, UTS, and ϵ_{UTS} . One-way analysis of variance was conducted to compare the mean of these mechanical properties for the LCL, RCL, and USL. The student's *t* test was used and the threshold chosen for statistical significance was 0.05. Data were analyzed using the JMP statistical software (JMP, Version 10, SAS Institute Inc.).

3. Results

3.1. SEM examination

Scanning electron micrographs of swine CL and USL cross-sections were obtained (Fig. 3). Collagen fibrils in both the CL (Fig. 3(a)) and USL (Fig. 3(c)) specimens appeared to be organized into bundles. These bundles were arranged primarily perpendicular to the ligaments' cross-sections and were more

loosely spaced in the CL than in the USL. The collagen fibrils were found to have a diameter of about 60–70 nm. In both ligaments, a loose network of individual collagen fibrils that intermingled with the collagen bundles was visible at high magnification (Fig. 3(b) and (d)). These collagen fibrils were oriented along random directions.

3.2. Histological examination

Presence of loose connective tissue was found in all the specimens with a larger amount of ground substance (in white) in the LCL specimen (Fig. 4(a) and (d)) and a larger amount of smooth muscle fibers and adipose cells (in white) in the RCL specimen (Fig. 4(c) and (f)). Loose connective tissue was also detected in the USL specimen. However, dense connective tissue, which is characterized by a considerable amount of collagen fibers and elastin fibers, was only identified in the USL specimen (Fig. 4(b) and (e)). The elastin content was significantly higher in the USL (Fig. 4(e)) than the CL (Fig. 4(d) and (f)).

Blood vessels were detected in all these ligaments (Fig. 5(a) and (d)). Details about their cross sections, such as the adventitia, media, and intima layers, were observed (Fig. 5(a)). The blood vessels were noticed to be primarily oriented perpendicular to the cross-section of the ligaments (Fig. 5(a) and (d)). Smooth muscle fiber bundles were also found to be arranged in the plane of the RCL and USL specimens (Fig. 5(b) and (e)). Nerve fibers had a similar arrangement and were detected in the USL and LCL specimens (Fig. 5(c) and (f)).

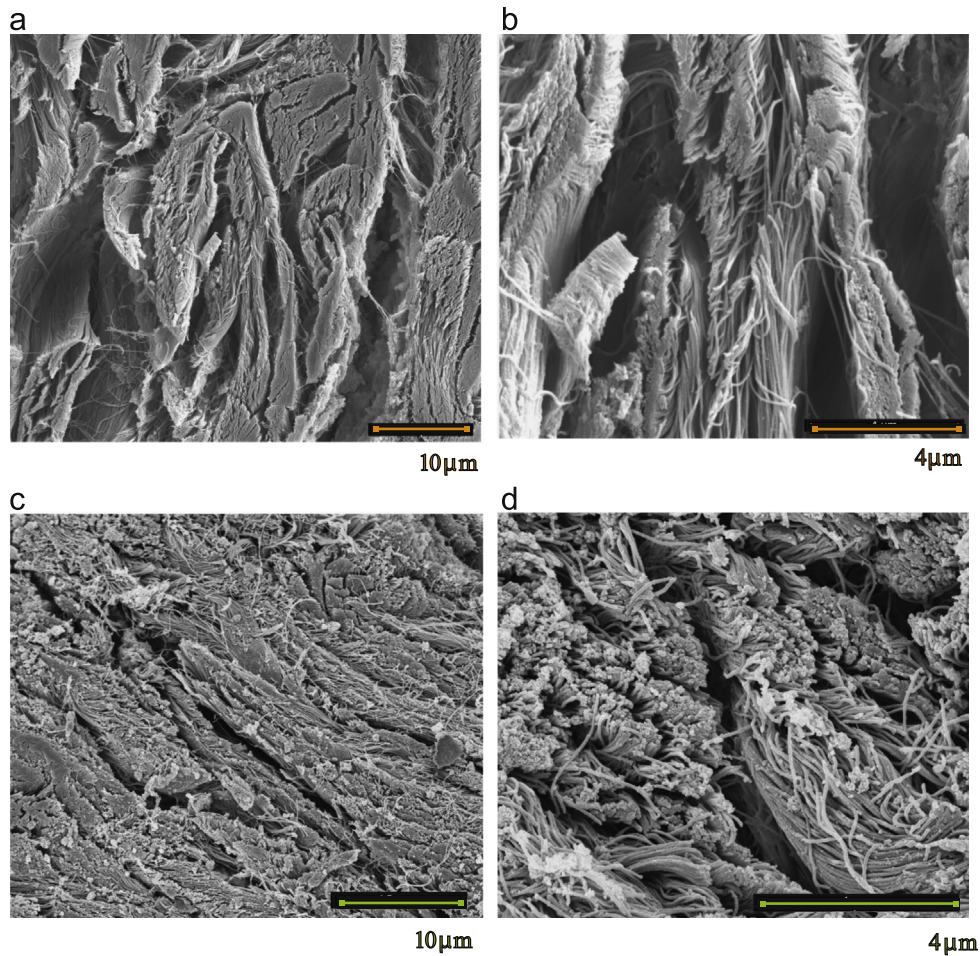


Fig. 3 – Scanning electron micrographs of swine CL cross section at (a) 5000 \times and (b) 20,000 \times magnifications and swine USL cross section at (c) 5000 \times and (d) 20,000 \times magnifications.

3.3. Tensile properties

The dimensions of the CL and USL specimens ($n=18$) obtained from one full term sow and used for mechanical testing are presented in Fig. 6. This figure presents a map indicating the location of each specimen relative to the cervix and rectum. The width (mean \pm std) was 7.455 ± 1.536 mm for the RCL, 7.457 ± 1.194 mm for the USL, and 8.489 ± 1.373 mm for the LCL. The thickness (mean \pm std) was 0.802 ± 0.135 mm for the RCL, 0.490 ± 0.086 mm for the USL and 1.119 ± 0.180 mm for the LCL. Axial stress–strain data obtained by testing these CL and USL specimens are presented in Fig. 7. The axial stress–strain response of the CL and USL displayed the nonlinear strain stiffening phenomenon which is characteristic of soft biological tissues. The tensile behavior of specimens collected from different regions within the USL/CL complex varied greatly.

The tangent moduli of the toe and linear regions of the stress–strain curve are plotted in Fig. 8 for each specimen. The values (mean \pm std) of the tangent moduli of the toe region of the stress–strain curve for the RCL, USL, and LCL were found to be 1.154 ± 0.786 MPa, 1.617 ± 1.215 MPa, 0.503 ± 0.396 MPa, respectively. The values (mean \pm std) of the tangent moduli of the

linear region for the RCL, USL, and LCL were found to be 5.385 ± 2.424 MPa, 29.816 ± 7.378 MPa, 3.449 ± 1.449 MPa, respectively. The results of the statistical analysis indicated that there was no significant difference in the tangent modulus of the toe or linear region between the RCL and LCL ($p>0.05$). Moreover, the tangent modulus of the toe region of the USL was determined to be significantly different from such modulus in the LCL ($p<0.05$) but not significantly different from such modulus in the RCL ($p>0.05$). However, the tangent modulus of the linear region for the USL was significantly different from the tangent modulus of such region for the RCL or LCL ($p<0.0001$).

The ultimate tensile strength (UTS) for each specimen is reported in Fig. 9(a). The values (mean \pm std) of the UTS for the RCL, USL, and LCL were found to be 1.278 ± 0.499 MPa, 2.767 ± 0.444 MPa, and 0.854 ± 0.207 MPa, respectively. The statistical analysis revealed that the UTS of the USL was significantly larger than the UTS of both the RCL and LCL ($p<0.0001$). The UTS of the LCL was not found to be significantly different from the UTS of the RCL ($p>0.05$). The axial strain measured at the UTS, ϵ_{UTS} , for each specimen is presented in Fig. 9(b). The values (mean \pm std) of ϵ_{UTS} for the RCL, USL, and LCL were determined to be 0.337 ± 0.166 , 0.216 ± 0.058 , and 0.424 ± 0.139 , respectively. No significant difference was observed between

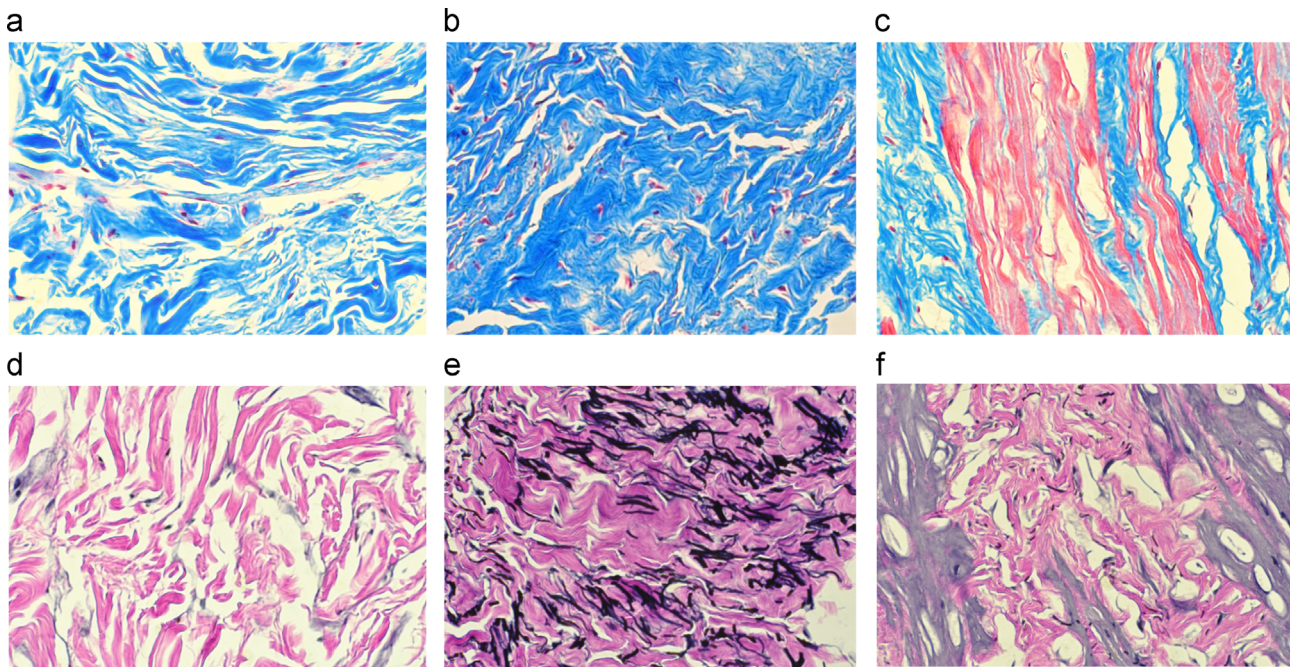


Fig. 4 – Histological images (40 × magnification) of longitudinal sections of swine (a) and (d) LCL, (b) and (e) USL, and (c) and (f) RCL. Masson's trichrome stain (blue = collagen, red = muscle and cytoplasm) is used for sections (a)–(c) and the Verhoeff–van Giesson stain (pink = collagen, purple = muscle, black = elastin and nuclei) for sections (d)–(f). (For interpretation of the references to color in this figure caption, the reader is referred to the web version of this paper.)

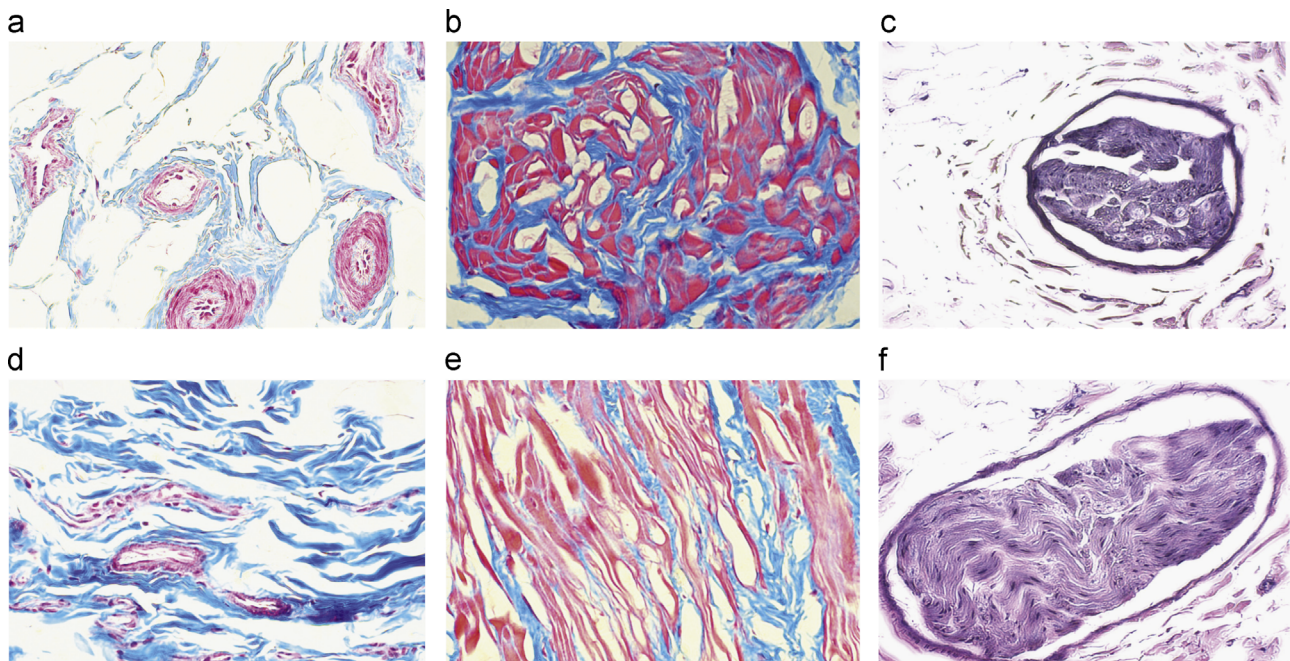


Fig. 5 – Histological images of cross sections (a)–(c) and longitudinal sections (d)–(f) of some components of the swine USL and CL: blood vessels (a) and (d), smooth muscle fibers (b) and (e), and nerve fibers (c) and (f). Masson's trichrome stain (blue = collagen, red = muscle and cytoplasm) is used for sections (a), (b), (d), and (e) and the Verhoeff–van Giesson stain (pink = collagen, purple = muscle, black = elastin and nuclei) for sections (c) and (f). (For interpretation of the references to color in this figure caption, the reader is referred to the web version of this paper.)

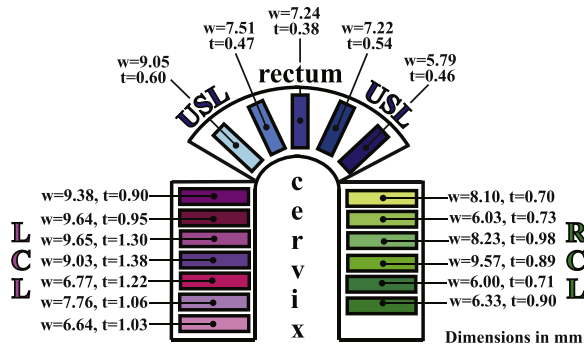


Fig. 6 – Width (*w*) and thickness (*t*) of LCL, USL, and RCL specimens.

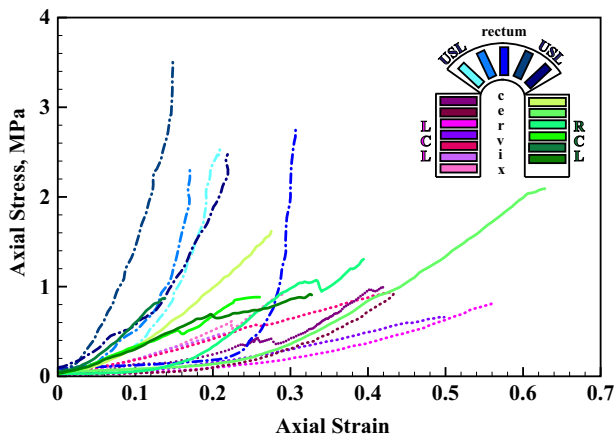


Fig. 7 – Axial stress–strain curves of the CL/USL complex of one full term sow. Three different symbols are used to report stress–strain data collected from specimens isolated from the three ligaments: RCL, USL and LCL. The different colors denote different specimen locations, within the CL/USL complex, relative to the cervix and rectum as shown in the insert. (For interpretation of the references to color in this figure caption, the reader is referred to the web version of this paper.)

the ϵ_{UTS} in the LCL and RCL ($p > 0.05$). However, the ϵ_{UTS} for the USL was significantly different from the ϵ_{UTS} for the LCL ($p < 0.05$) but not significantly different from the ϵ_{UTS} for the RCL ($p > 0.05$).

4. Discussion

This study focuses on determining the structural and mechanical properties of two major ligaments, the CL and USL, of the uterus–cervix–vagina complex using the swine as animal model. The structural composition of these ligaments was determined by performing histological and SEM analyses. Tensile tests on CL and USL specimens were conducted and the tangent moduli of the toe and linear regions of the stress–strain curves, UTS, and strain at the UTS, ϵ_{UTS} , were computed. The histological, SEM, and mechanical data revealed significant differences between the CL and USL. Due to existing similarities between the histological properties of the swine and human CL and USL (Gruber et al., 2011), this investigation

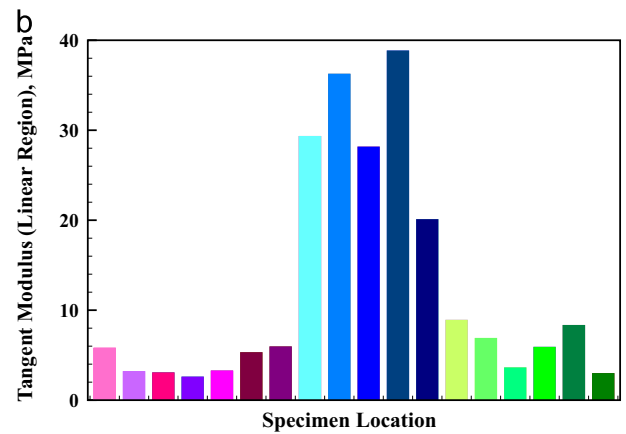
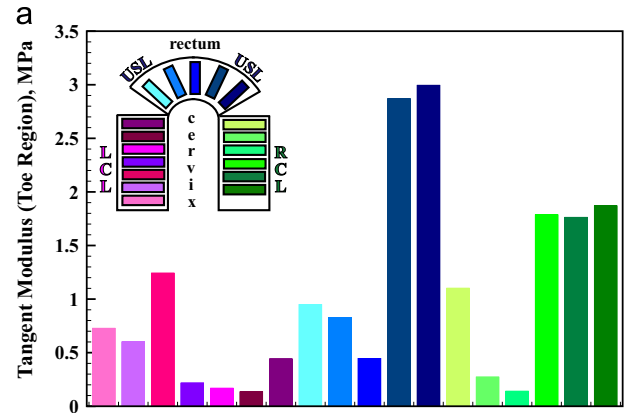


Fig. 8 – Tangent modulus of (a) toe region and (b) linear region of stress–strain curves obtained by testing $n = 18$ specimens. Different colors denote specimen locations, within the CL/USL complex, relative to the cervix and rectum as shown in the insert. (For interpretation of the references to color in this figure caption, the reader is referred to the web version of this paper.)

provides crucial information on the material behavior of the supportive structures of the female pelvic floor.

The SEM analysis indicates that the collagen fibers were disorganized but mainly oriented in the *in-vivo* loading direction of the CL and USL. In the swine, the collagen fibers were more densely packed in the USL than in the CL (Fig. 3(b) and (d)). The presence of collagen fibers, elastin fibers, smooth muscle, adipose tissues, nerve fibers, and blood vessels in the swine CL and USL was also reported in human CL and USL (Ramanah et al., 2012), thus supporting our choice to use the swine as an animal model for mechanical testing. The composition of the CL and USL in the swine was similar but with some significant differences (Fig. 4). Both these ligaments contained mainly collagen in the swine (Gabriel et al., 2005) (as in humans, Ewies et al., 2003). The amount of elastin in the USL was significantly greater than that found in the CL. Dense connective tissue was only detected in the USL. Loose connective tissues were abundant in both the LCL and RCL. In the LCL, ground substance and nerve fibers were the most abundant whereas, in the RCL, ground substance, adipose cells, and smooth muscle cells were more prevalent. It must be noted that these results were obtained by analyzing a few representative sections of the whole ligaments in pregnant

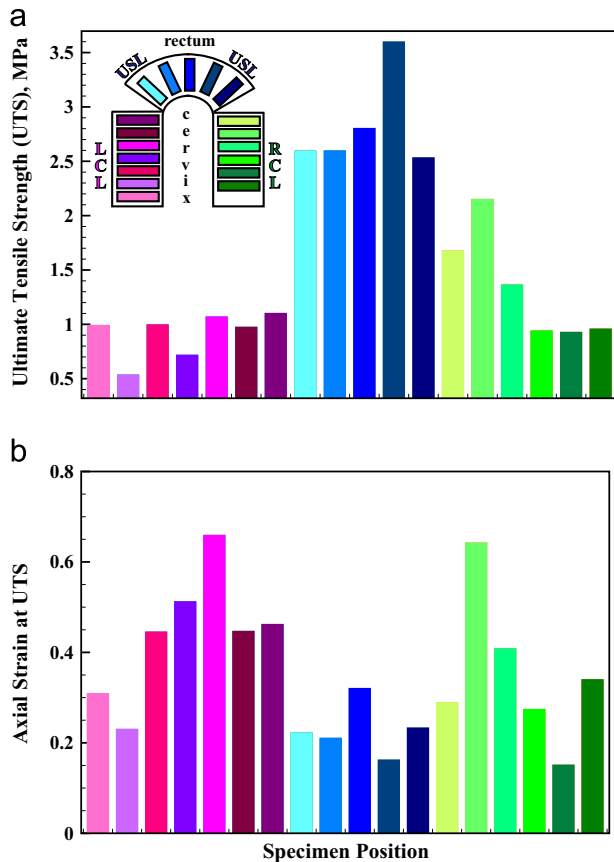


Fig. 9 – (a) Ultimate tensile strength (UTS) and (b) strain at the UTS of $n=18$ specimens. Different colors denote specimen locations, within the CL/USL complex, relative to the cervix and rectum as shown in the insert. (For interpretation of the references to color in this figure caption, the reader is referred to the web version of this paper.)

swine so one must be cautious in generalizing them. Indeed, the compositional difference between the LCL and RCL observed in our study may be caused by a possible selection of neural sections for the LCL and vascular sections for the RCL for our histological analysis (Ramanah et al., 2012).

The results of the mechanical tests revealed that the uniaxial stress–strain response of the CL/USL complex strongly depends on specimen location, although the qualitative response of specimens within the LCL, RCL, or USL was similar (Fig. 7). The USL exhibited a significantly larger tangent modulus in the linear region (Fig. 8(b)) and larger UTS (Fig. 9(a)) than the CL while the strain at the UTS, ϵ_{UTS} , was significantly lower (Fig. 9). These differences could be attributed to the different composition and structure of the ligaments. The higher tangent modulus in the linear region and strength of the USL were to be expected given their content of dense connective tissue (Fig. 5(b)–(e)). Because the collagen fibers were oriented mainly along the loading direction in the USL, the mechanical failure was likely determined by the simultaneous rather than progressive failure of the comprising fibers. Such failure mechanisms could explain the lower strain at the UTS for the USL.

Stress–strain curves are presented only up to the UTS in Fig. 7. Local maxima were observed in the stress–strain curves of some CL specimens. These local maxima were

due to partial thickness tears of the loose connective tissues (Fig. 4(a), (c), (d), and (f)). It must be noted that, despite the tears, the CL specimens continued to carry increasing loads as they were stretched. Interestingly, there were local maxima in the stress–strain curve at strain larger than ϵ_{UTS} for both of the USL and the CL (data not reported). The ability of the USL and CL complex to sustain tears and continue to support significant loads is a mechanical feature that warrants further investigation in the future.

Different experimental protocols have been used to investigate the elastic properties of human and animal USLs (Vardy et al., 2005; Martins et al., 2013; Rivaux et al., 2013). Vardy et al. (2005) conducted incremental stress relaxation tests followed by tensile tests up to failure on USLs in monkeys. They reported a strain-dependent elastic modulus on the order of several hundreds to several thousands of kilopascals and a mean failure stress of 0.6 MPa. Martins et al. (2013) found that the mean elastic modulus and UTS of USLs collected from female cadavers via uniaxial tensile tests were 14.1 MPa and 6.3 MPa, respectively. Similarly, Rivaux et al. (2013) performed uniaxial tensile tests on USLs of female cadavers and reported a mean UTS of 4 MPa.

In this study, we identified a mean elastic modulus of 1.6 MPa in the toe region and 29.8 MPa in the linear region and a mean ultimate stress of 2.8 MPa for the swine USL. These values are of the same order of magnitude than those reported in the literature (Vardy et al., 2005; Martins et al., 2013). However, major differences in the results may exist due to differences between our experimental methods and previously used ones. Due to the large size of the swine ligaments, we were able to prepare specimens with an aspect ratio significantly larger (at least 5:1) than those used in the work by Vardy et al. (2005) and Martins et al. (2013). Moreover, in the aforementioned studies, engineering strain was reported and its measurement was based on the displacement of the clamps of the uniaxial testing system. In our study, the Lagrangian strain was computed by video-tracking the motion of markers attached to the specimens. We believe that the high aspect ratio of the test specimens and optical technique used to determine the Lagrangian strain provide experimental data that more accurately characterize the tensile properties of the USL and CL (Abramowitch et al., 2009).

Non-human primates have the pelvic anatomy that is most similar to humans (Rosenberg and Trevathan, 2002). Despite this advantage, the low availability and high expense in maintaining a primate colony has led us to seek a more cost effective animal model to study the mechanical properties of the supportive structures of the pelvic organs. The use of a large animal model such as the swine can help in reducing variation in the measurement of mechanical properties since multiple test specimens can be collected from a single animal. In order to determine the extent to which our mechanical studies can be generalized to humans, additional micro-structural analyses and mechanical experiments are needed on both the swine and human CL and USL. Because humans are bipeds and swine are quadrupeds, their pelvic floors are remarkably different. Nevertheless, our results seem to suggest that the histology and mechanical properties of the swine CL and USL are very similar to those in humans. In light of this evidence, we believe that the swine may be a

practical animal model for pelvic floor research, especially since it naturally develops pelvic floor disorder such as prolapse (Gruber et al., 2011; Couri et al., 2012).

Acknowledgments

Funding was provided by NSF CAREER Grant no. 1150397. The authors would like to thank Susan Nicewonder for her help with the dissection.

REFERENCES

- Abramowitch, S.D., Feola, A., Jallah, Z., Moalli, P.A., 2009. Tissue mechanics, animal models, and pelvic organ prolapse: a review. *Eur. J. Obstet. Gynecol. Reprod. Biol.* 144, 146–158.
- Amundsen, C.L., Flynn, B.J., Webster, G.D., 2003. Anatomical correction of vaginal vault prolapse by uterosacral ligament fixation in women who also require a pubovaginal sling. *J. Urol.* 169, 1770–1774.
- Becker, W.R., De Vita, R., 2014. Biaxial mechanical properties of swine uterosacral and cardinal ligaments. *Biomech. Model. Mechanobiol.* <http://dx.doi.org/10.1007/s10237-014-0621-5>.
- Buller, J.L., Thompson, J.R., Cundiff, G.W., Sullivan, L.K., Schön Ybarra, M.A., Bent, A.E., 2001. Uterosacral ligament: description of anatomic relationships to optimize surgical safety. *Obstet. Gynecol.* 97, 873–879.
- Chen, B.H., Wen, Y., Li, H., Polan, M.L., 2002. Collagen metabolism and turnover in women with stress urinary incontinence and pelvic prolapse. *Int. Urogynecol. J.* 13, 80–87.
- Cosson, M., Boukerrou, M., Lacaze, S., Lambaudie, E., Fasel, J., Mesdagh, H., Lobry, P., Ego, A., 2003. A study of pelvic ligament strength. *Eur. J. Obstet. Gynecol. Reprod. Biol.* 109, 80–87.
- Couri, B.M., Lenis, A.T., Borazjani, A., Paraiso, M.F.R., Damaser, M.S., 2012. Animal models of female pelvic organ prolapse: lessons learned. *Expert Rev. Obstet. Gynecol.*, 249–260.
- DeLancey, J.O.L., 1994. The anatomy of the pelvic floor. *Curr. Opin. Obstet. Gynecol.* 6, 313–336.
- Ewies, A.A.A., Al-Azzawi, F., Thompson, J., 2003. Changes in extracellular matrix proteins in the cardinal ligaments of post-menopausal women with or without prolapse: a computerized immunohistomorphometric analysis. *Hum. Reprod.* 18, 2189–2195.
- Gabriel, B., Denschlag, D., Göbel, H., Fittkow, C., Werner, M., Gitsch, G., Watermann, D., 2005. Uterosacral ligament in postmenopausal women with or without pelvic organ prolapse. *Int. Urogynecol. J.* 16, 475–479.
- Goepel, C., 2008. Differential elastin and tenascin immunolabeling in the uterosacral ligaments in postmenopausal women with and without pelvic organ prolapse. *Acta Histochem.* 110, 204–209.
- Gruber, D.D., Warner, W.B., Lombardini, E.D., Zahn, C.M., Buller, J.L., 2011. Anatomical and histological examination of the porcine vagina and supportive structures: in search of an ideal model for pelvic floor disorder evaluation and management. *Female Pelvic Med. Reconstr. Surg.* 17, 110–114.
- Kenton, K., Mueller, E.R., 2006. The global burden of female pelvic floor disorders. *BJU Int.* 98, 1–5.
- Kepenekci, I., Keskinilic, B., Akinsu, F., Cakir, P., Elhan, A.H., Erkek, A.B., Kuzu, M.A., 2011. Prevalence of pelvic floor disorders in the female population and the impact of age, mode of delivery, and parity. *Dis. Colon Rectum* 54, 85–94.
- Lowder, J.L., Debes, K.M., Moon, D.K., Howden, N., Abramowitch, S.D., Moalli, P.A., 2007. Biomechanical adaptations of the rat vagina and supportive tissues in pregnancy to accommodate delivery. *Obstet. Gynecol.* 109, 136–143.
- Luo, J., Smith, T.M., Ashton-Miller, J.A., DeLancey, J.O.L., 2014. In vivo properties of uterine suspensory tissue in pelvic organ prolapse. *J. Biomech. Eng.* 136, 021016.
- MacLennan, A.H., Taylor, A.W., Wilson, D.H., Wilson, D., 2000. The prevalence of pelvic floor disorders and their relationship to gender, age, parity and mode of delivery. *BJOG* 107, 1460–1470.
- Martins, P., Silva-Filho, A.L., Fonseca, A.M.R.M., Santos, A., Santos, L., Mascarenhas, T., Jorge, R.M.N., Ferreira, A.M., 2013. Strength of round and uterosacral ligaments: a biomechanical study. *Arch. Gynecol. Obstet.* 287, 313–318.
- Miklos, J.R., Moore, R.D., Kohli, N., 2002. Laparoscopic surgery for pelvic support defects. *Curr. Opin. Obstet. Gynecol.* 14, 387–395.
- Moalli, P.A., Howden, N.S., Lowder, J.L., Navarro, J., Debes, K.M., Abramowitch, S.D., Woo, S.L.Y., 2005. A rat model to study the structural properties of the vagina and its supportive tissues. *Am. J. Obstet. Gynecol.* 192, 80–88.
- Mokrzycki, M.L., Mittal, K., Smilen, S.W., Blechman, A.N., Porges, R.F., Demopolous, R.I., 1997. Estrogen and progesterone receptors in the uterosacral ligament. *Obstet. Gynecol.* 90, 402–404.
- Petros, P.E., 2010. *The Female Pelvic Floor: Function, Dysfunction and Management According to the Integral Theory*. Springer Verlag, Berlin, Heidelberg, New York.
- Ramanah, R., Berger, M.B., Parratte, B.M., DeLancey, J.O.L., 2012. Anatomy and histology of apical support: a literature review concerning cardinal and uterosacral ligaments. *Int. Urogynecol. J.* 23, 1483–1494.
- Reay Jones, N.H.J., Healy, J.C., King, L.J., Saini, S., Shousha, S., Allen-Mersh, T.G., 2003. Pelvic connective tissue resilience decreases with vaginal delivery, menopause and uterine prolapse. *Br. J. Surg.* 90, 466–472.
- Rivaux, G., Rubod, C., Dedet, B., Brieu, M., Gabriel, B., Cosson, M., 2013. Comparative analysis of pelvic ligaments: a biomechanics study. *Int. Urogynecol. J.* 24, 135–139.
- Rosenberg, K., Trevathan, W., 2002. Birth, obstetrics and human evolution. *BJOG* 109, 1199–1206.
- Sherwood, O.D., 2004. Relaxin's physiological roles and other diverse actions. *Endocr. Rev.* 25, 205–234.
- Subak, L.L., Waetjen, L.E., van den Eeden, S., Thom, D.H., Vittinghoff, E., Brown, J.S., 2001. Cost of pelvic organ prolapse surgery in the United States. *Obstet. Gynecol.* 98, 646–651.
- Vardy, M.D., Gardner, T.R., Cosman, F., Scotti, R.J., Mikhail, M.S., Preiss-Bloom, A.O., Williams, J.K., Cline, J.M., Lindsay, R., 2005. The effects of hormone replacement on the biomechanical properties of the uterosacral and round ligaments in the monkey model. *Am. J. Obstet. Gynecol.* 192, 1741–1751.
- Weber, A.M., Buchsbaum, G.M., Chen, B., Clark, A.L., Damaser, M.S., Daneshgari, F., Davis, G., DeLancey, J., Kenton, K., Weidner, A.C., Word, R.A., 2004. Basic science and translational research in female pelvic floor disorders: proceedings of an NIH-sponsored meeting. *Neurourol. Urodyn.* 23, 288–301.
- Wu, J.M., Hundley, A.F., Fulton, R.G., Myers, E.R., 2009. Forecasting the prevalence of pelvic floor disorders in U.S. women: 2010 to 2050. *Obstet. Gynecol.* 114, 1278–1283.